Supporting Information

Ultra-Durable and Transparent Self-Cleaning Surfaces by Large-Scale Self-Assembly of Hierarchical Interpenetrated Polymer Networks

William S.Y. Wong[1], *Zbigniew H. Stachurski*[2], *David R. Nisbet*[3], *Antonio Tricoli*[1]*

[1] Nanotechnology Research Laboratory, Research School of Engineering, The Australian National University, Canberra ACT 2601, Australia

[2] Research School of Engineering, The Australian National University, Canberra ACT 2601, Australia

[3] Laboratory of Advanced Biomaterials, Research School of Engineering, The Australian National University, Canberra ACT 2601, Australia

*Corresponding author: Dr. Antonio Tricoli
e-mail: antonio.tricoli@anu.edu.au
Tel: +61 2 6125 1696

Table S1. Comparative performance with robust superhydrophobic coatings in the literature.

Material	Transmittance Losses (600 nm)	Abrasion Test	Abrasion Resistance[#]	UV-Resistance	Acid-Resistance	Ref.
PU-PMMA IPN-$FSiO_2$	15 %	ASTM D4060, Rotary Abrasion	300 cycles	≥ 50 h, 254 nm, 3.3 mW/cm^2	≥ 24 h, 1M HCl	This work
Fluoro-diatoms	N.A	ASTM D4060, Rotary Abrasion	200 cycles	N.A	N.A	[17]
Flame-spray TiO_2/SiO_2	N.A	ASTM D4060, Rotary Abrasion	2-5 cycles	N.A	N.A	[13]
BOSTIK-$FTiO_2$	Not transparent	Sandpaper Abrasion Test (240 grit), 100 g mass	≥ 40 cycles	N.A	N.A	[5]
Acrylic-urethane-$FSiO_2$	Not transparent	Sandpaper Abrasion Test (2000 mesh), 2 kPa	200 cycles	N.A	≥ 12 h, HCl, pH 1	[16]
Templated PU	N.A	Polished Aluminum Rubbing Test (3 kPa)	10,000 cycles	N.A	N.A	[19]
Silicone-F (oxides)	0-10 %	Water test	Water jet, 45 kPa	N.A	N.A	[9]
F-SiO_2	< 5 %	Water test	Water rinse	N.A	N.A	[11]
PU-$FSiO_2$	0-10 %	N.A	N.A	200-400 h, UV-A	N.A	[12]
$FSiO_2$-ZnO nanorods	0-10 %	N.A	N.A	≥ 300 min, 365 nm, 2 mW/cm^2	N.A	[32]
F-BiOCl	N.A	N.A	N.A	≥ 270 min, 254 – 365 nm	N.A	[37]

– Until loss of 150° CA.

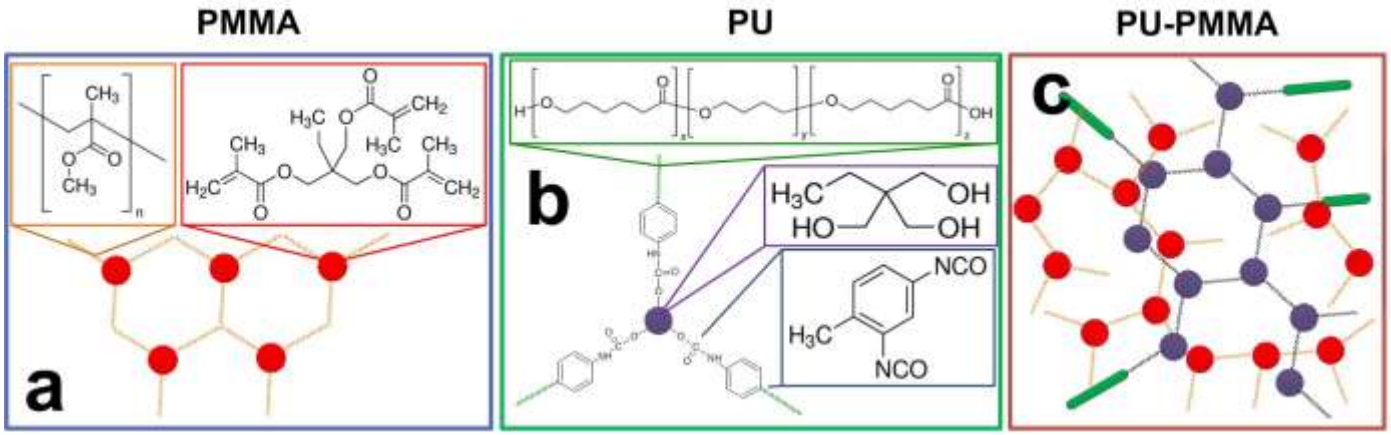

Figure S1. Molecular schematic of (a) crosslinked PMMA, (b) crosslinked PU and the optimally developed (c) PU-PMMA Interpenetrated Polymer Networks (IPNs).

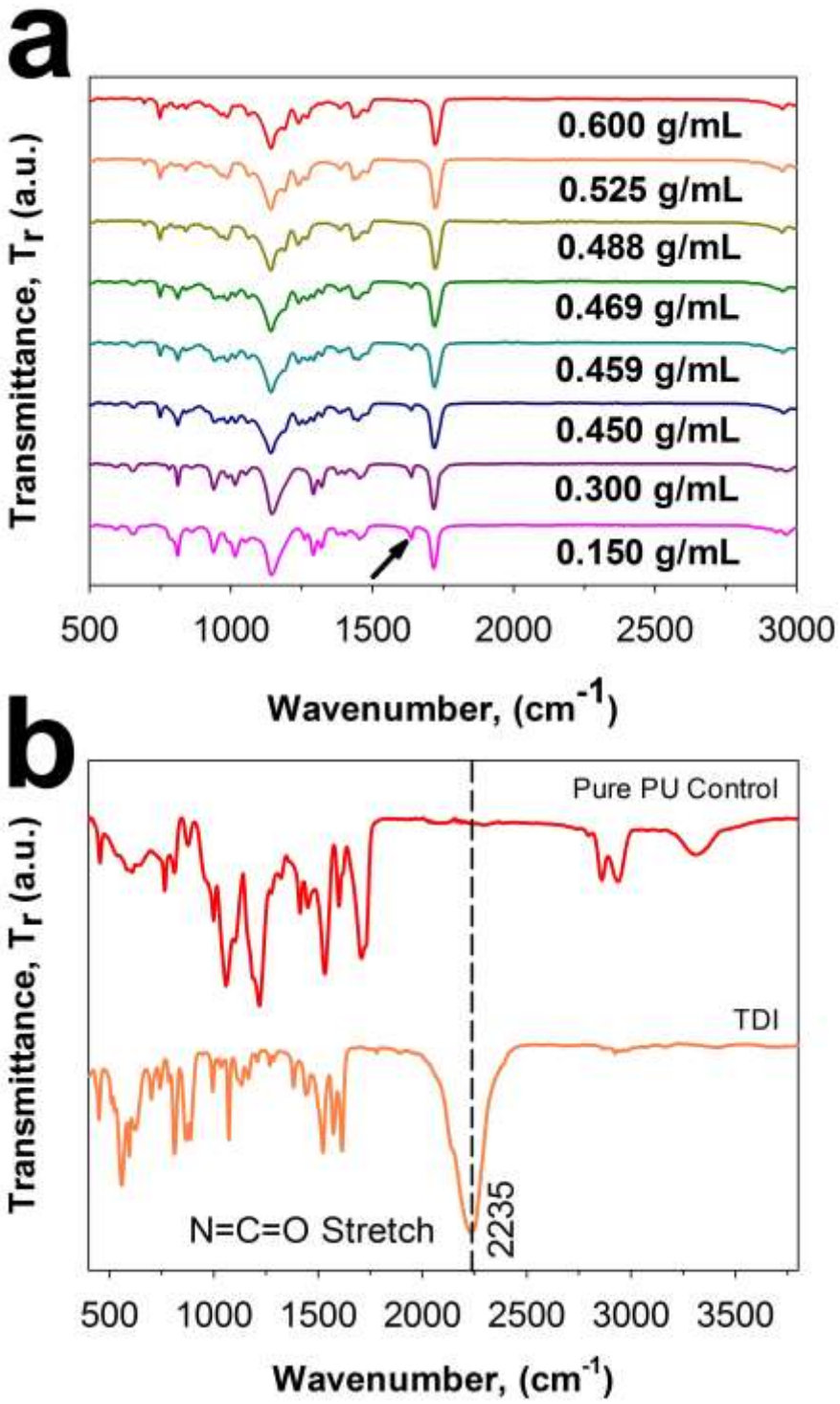

Figure S2. Development of optimal controls – cross-linked PU and PMMA. (a) Spectroscopic analysis of optimal PMMA control developed at a polymer to solvent ratio of 0.450 g/mL, which revealed only partial reaction of C=C 1637 cm^{-1} stretch, while preserving sprayability (primary comparative property in this work). (b) Spectroscopic analysis of optimal PU control developed at a polymer to solvent ratio of 0.075 g/mL, which revealed complete reaction of the isocyanate group at 2235 cm^{-1} and 3227 cm^{-1} and 3492 cm^{-1} – OH stretches belonging to PTHF and TRIOL respectively while forming the 3300 cm^{-1} –NH stretch, indicating complete formation of the cross-linked polymer.

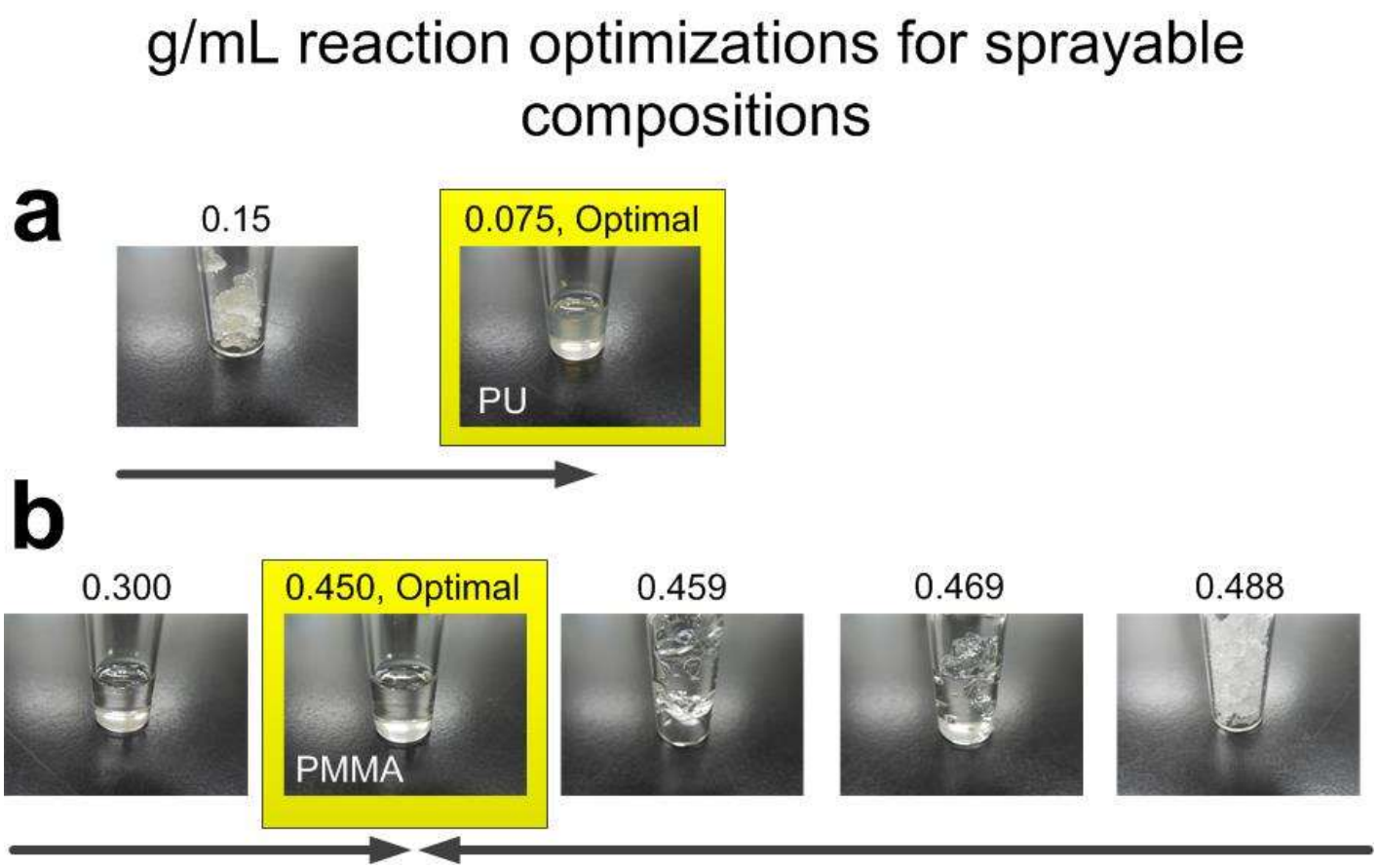

Figure S3. Optical photographs of optimized sprayable (a) PU and (b) PMMA crosslinked controls. It is notable that purely cross-linked PMMA developed in this solvent system (xylene:acetone), were not sprayable (See b, 0.488 – 0.600 polymer to solvent ratios).

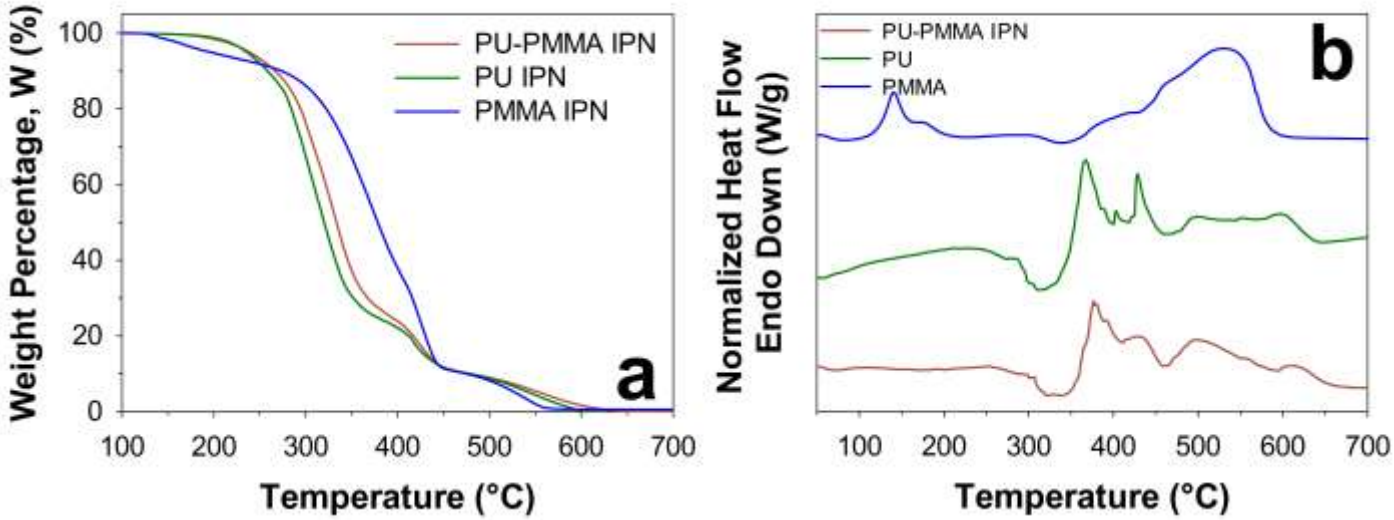

Figure S4. High temperature (a) thermogravimetric- (b) differential scanning calorimetric (TG-DSC) analysis of cross-linked PU, PMMA and PU-PMMA IPNs.

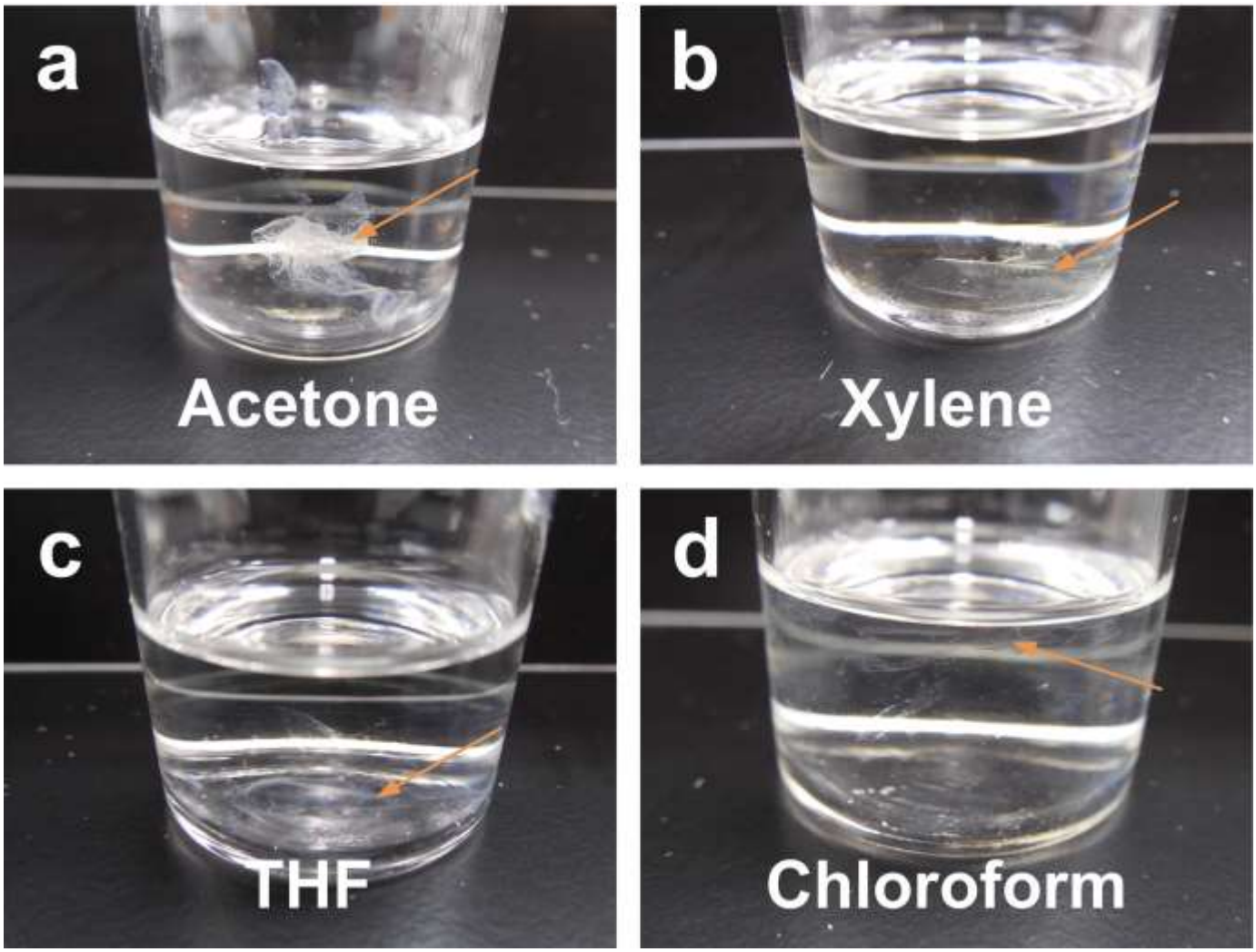

Figure S5. Determination of successfully synthesized interpenetrated networks (PU-PMMA IPN) through solvent-immersion tests over 2 h (and re-observed over 24 h with negligible differences). Thin films were notably not soluble in (a,b) parent solvents (acetone, xylene) while being swelled significantly in much (c,d) stronger solvents (THF and chloroform). Polymer coatings are indicated with orange arrows.

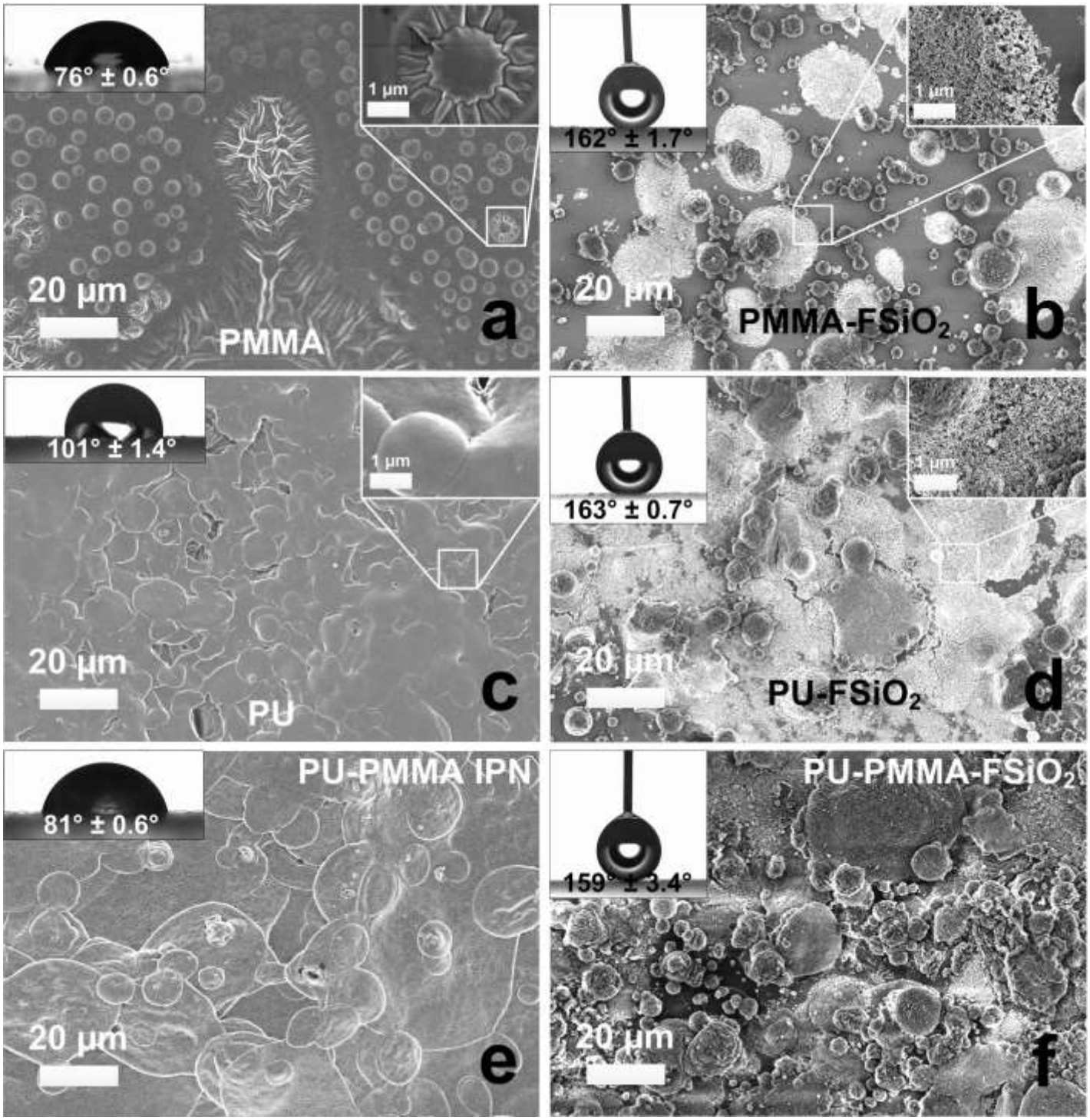

Figure S6. SEM analysis of crosslinked (a) PMMA, (c) PU and (e) PU-PMMA IPNs before (a,c,e) and after integration with the (b,d,f) F-SiO_2 coating.

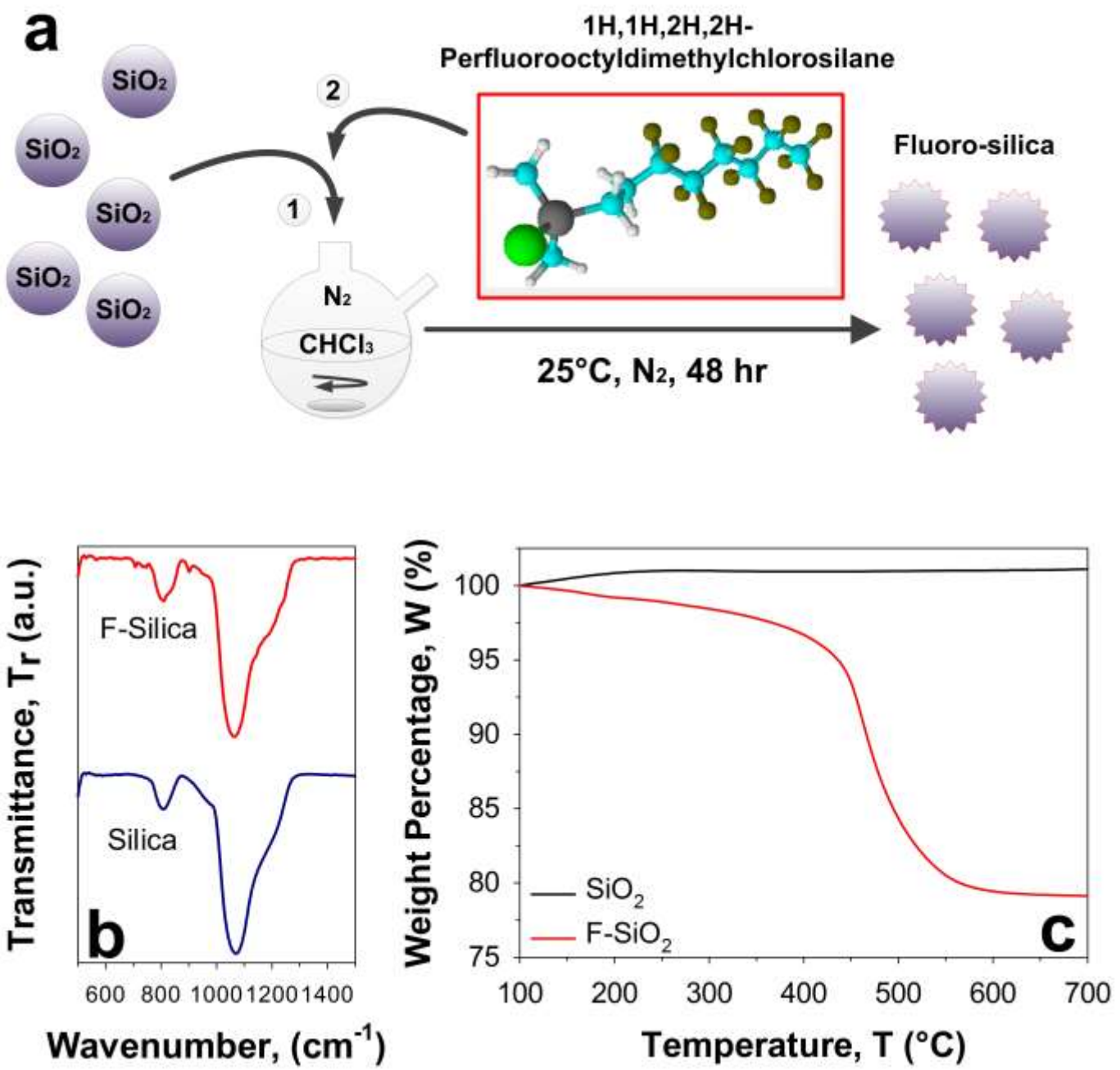

Figure S7. (a) Functionalization of silica with 1H,1H,2H,2H-Perfluorooctyldimethylchlorosilane, forming fluoro-silica, with (b) additional organic signatures as highlighted in IR-spectroscopy. Functionalization was further confirmed by (c) thermogravimetric analysis of the functionalized vs. control silica.

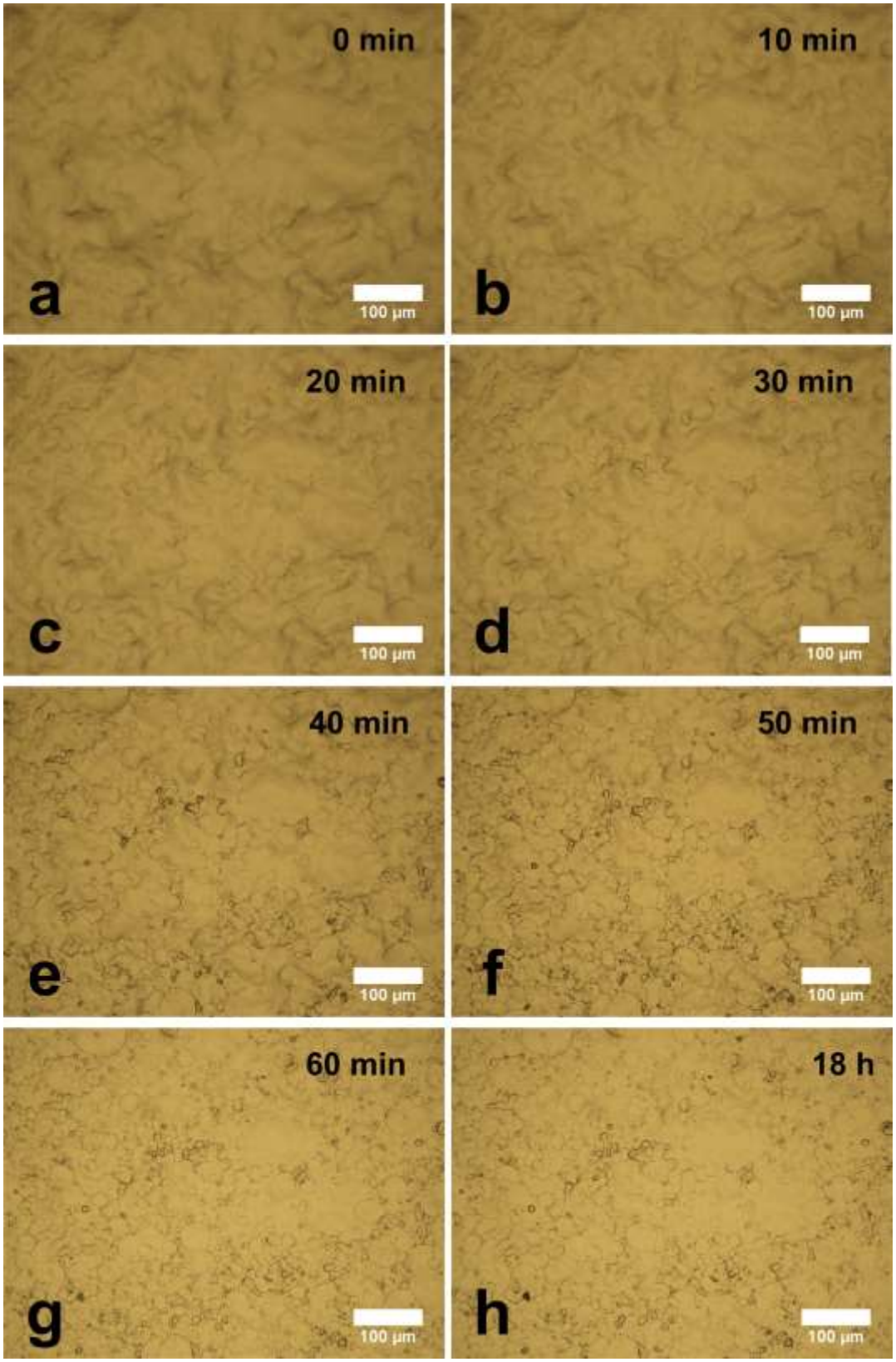

Figure S8. Optimization of VOC degassing (25 °C in a laboratory environment (50-60% humidity)), kept out of direct sunlight) analyzed through optical microscopy from 0 min to 18 h. Biggest morphological changes from an agglomerated coating (0 mins) to a micro-textured coating (marshmallow-like) took place between 20 to 40 min, in close alignment with the optimal timeframe for degassing-abrasion studies.

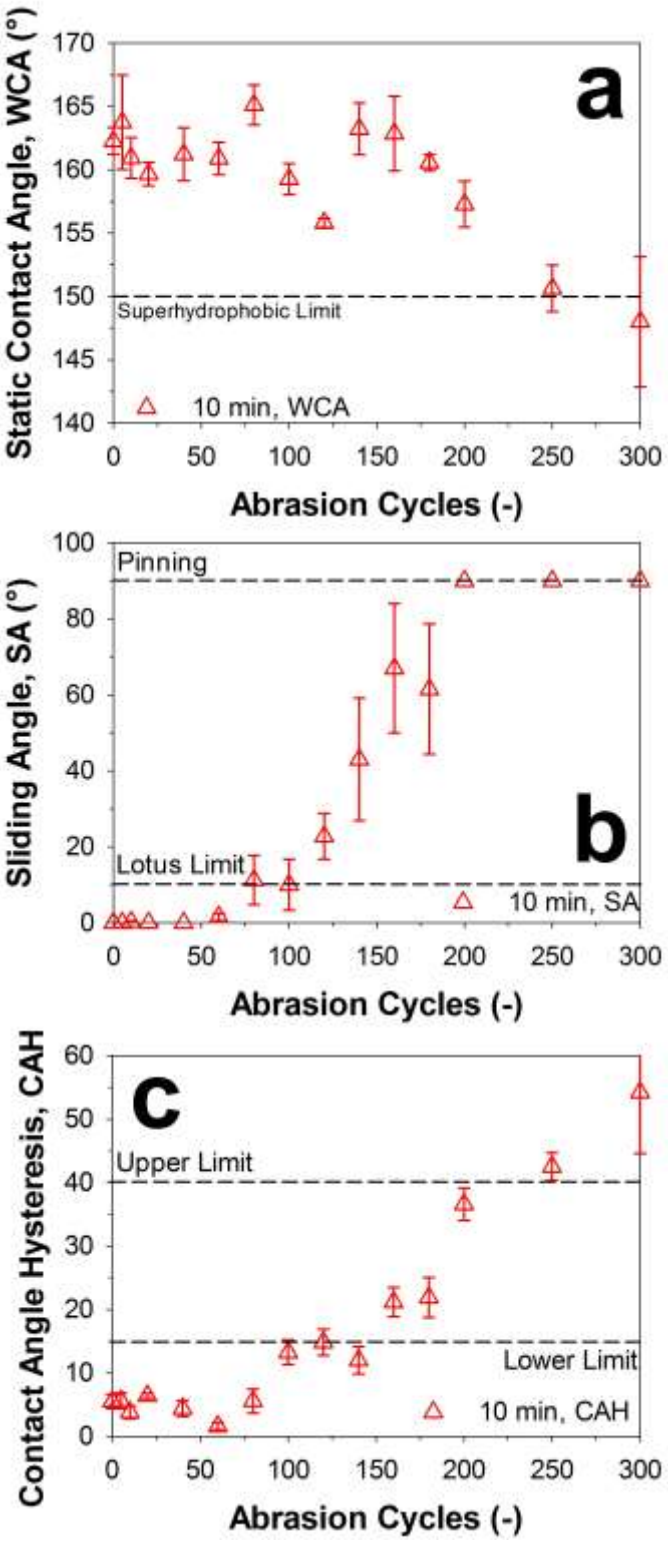

Figure S9. Isolated graphs demonstrating time-optimized abrasion-wetting characterizations. (a) WCAs, (b) SAs, (c) CAHs. Lag time for VOC degassing prior to nanoparticle deposition at 10 min.

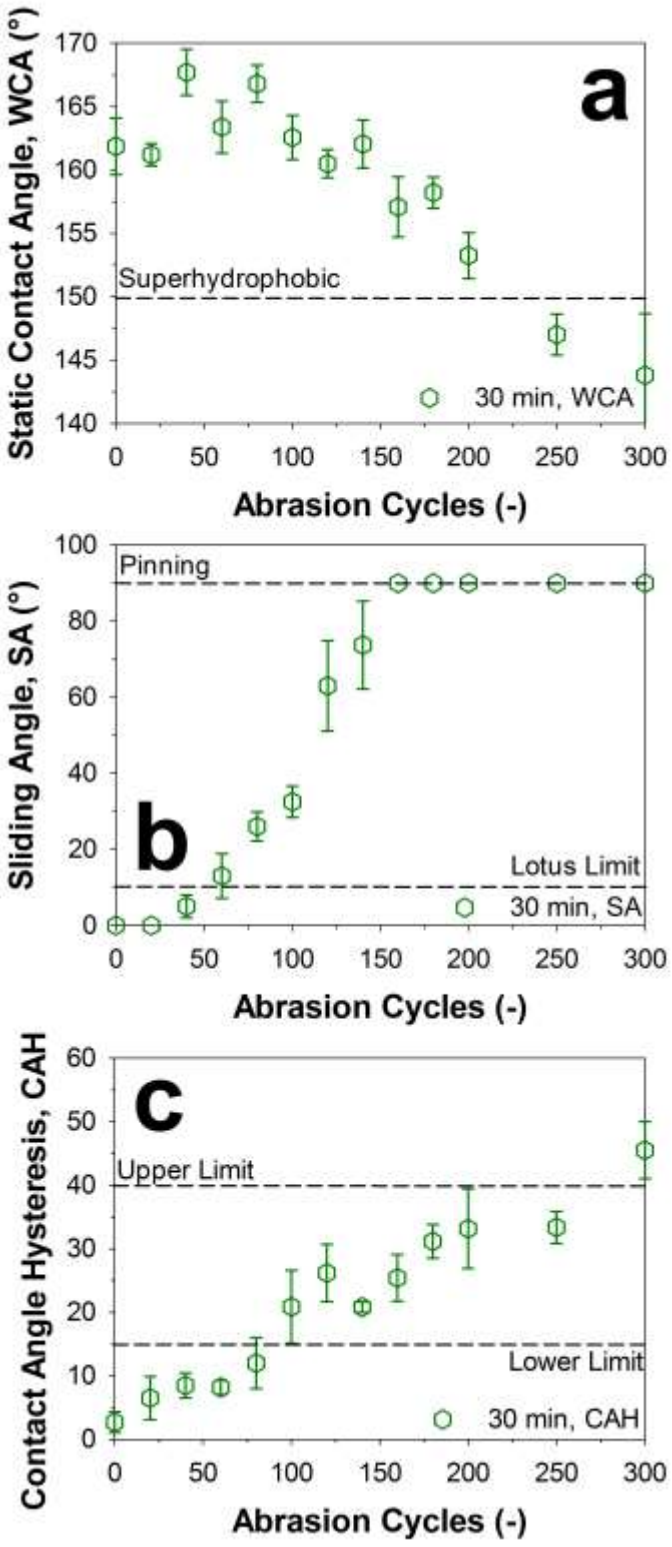

Figure S10. Isolated graphs demonstrating time-optimized abrasion-wetting characterizations. (a) WCAs, (b) SAs, (c) CAHs. Lag time for VOC degassing prior to nanoparticle deposition at 30 min.

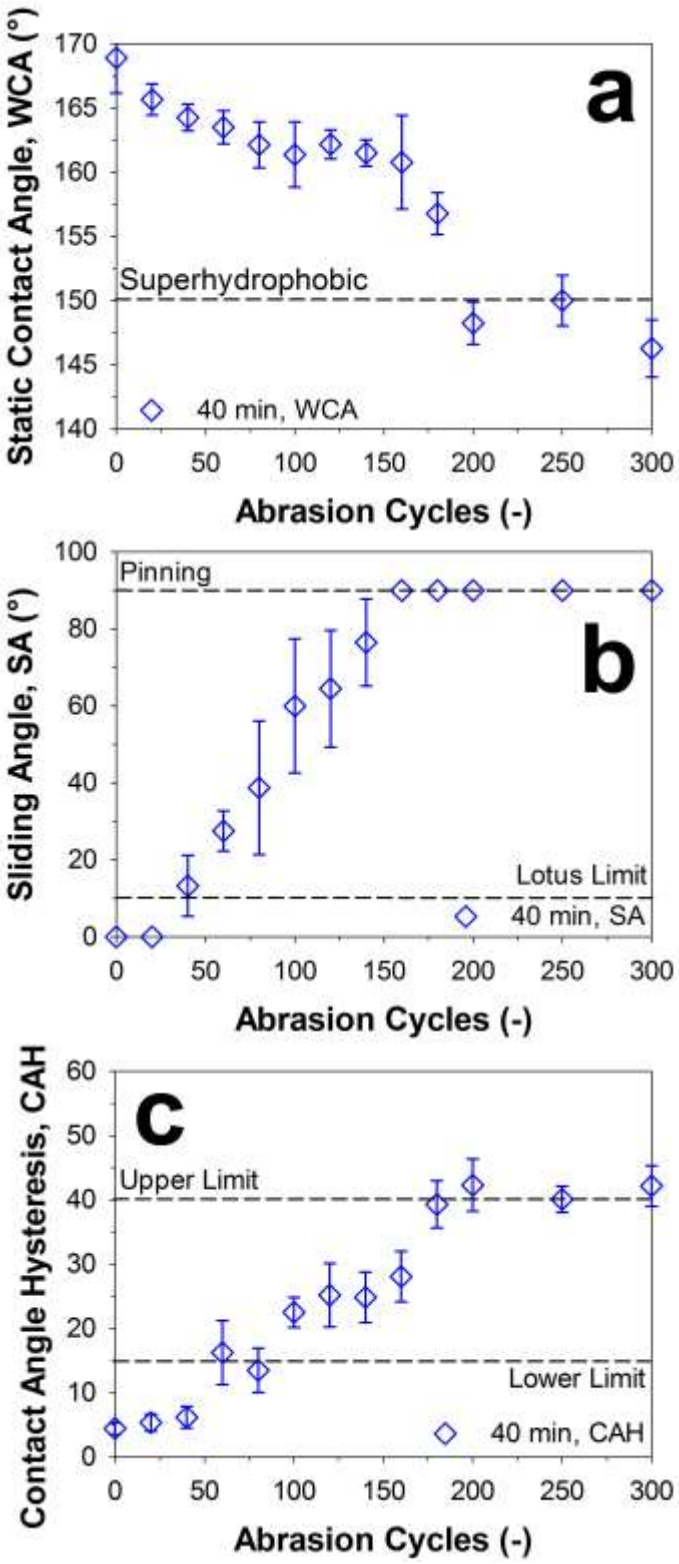

Figure S11. Isolated graphs demonstrating time-optimized abrasion-wetting characterizations. (a) WCAs, (b) SAs, (c) CAHs. Lag time for VOC degassing prior to nanoparticle deposition at 40 min.

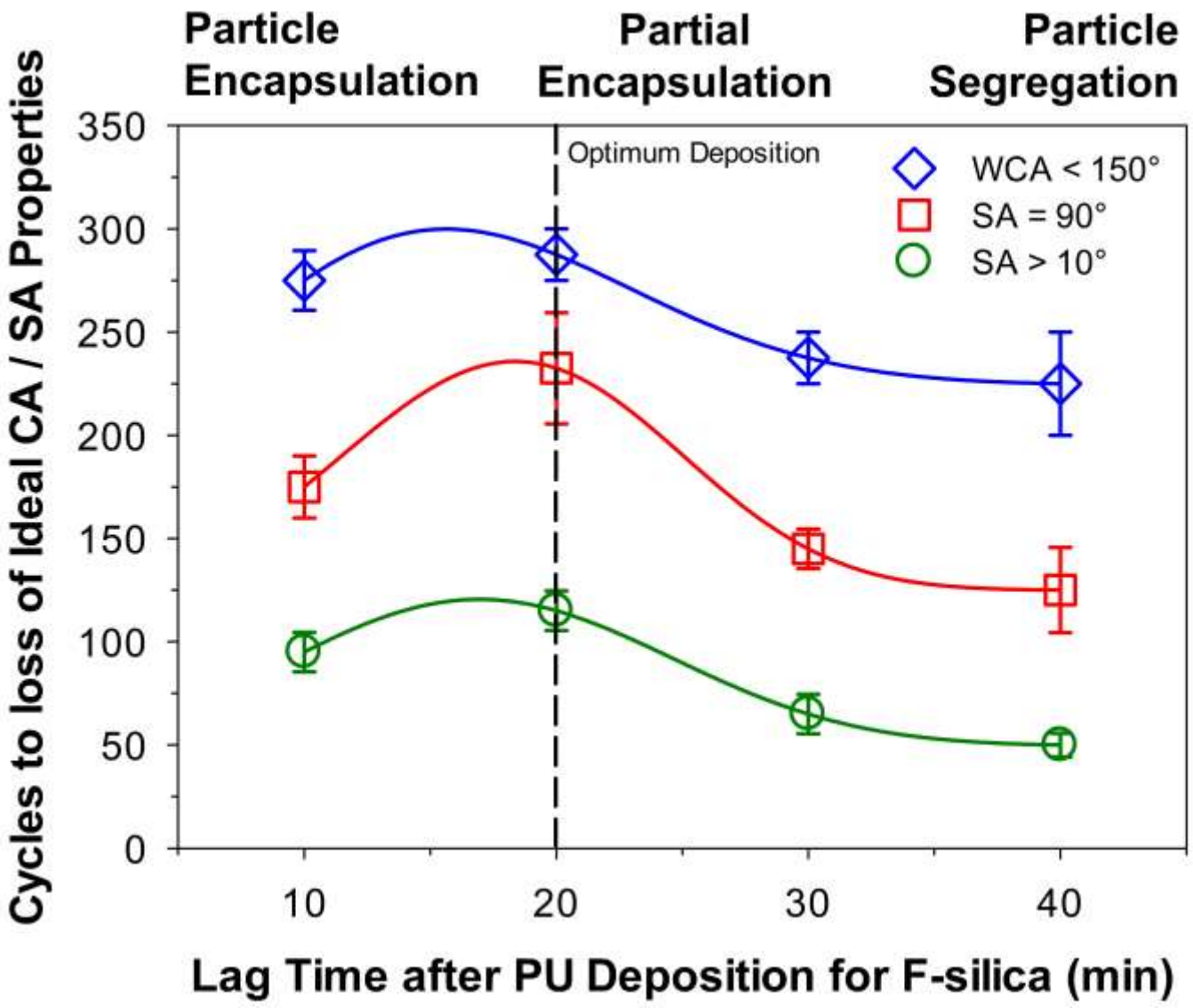

Figure S12. Optimization of VOC degassing analyzed through abrasion testing from 10 to 40 min, with a focus on WCA, SA and CAH properties. At < 10 min (e.g. 5 min), as-developed coatings were not superhydrophobic.

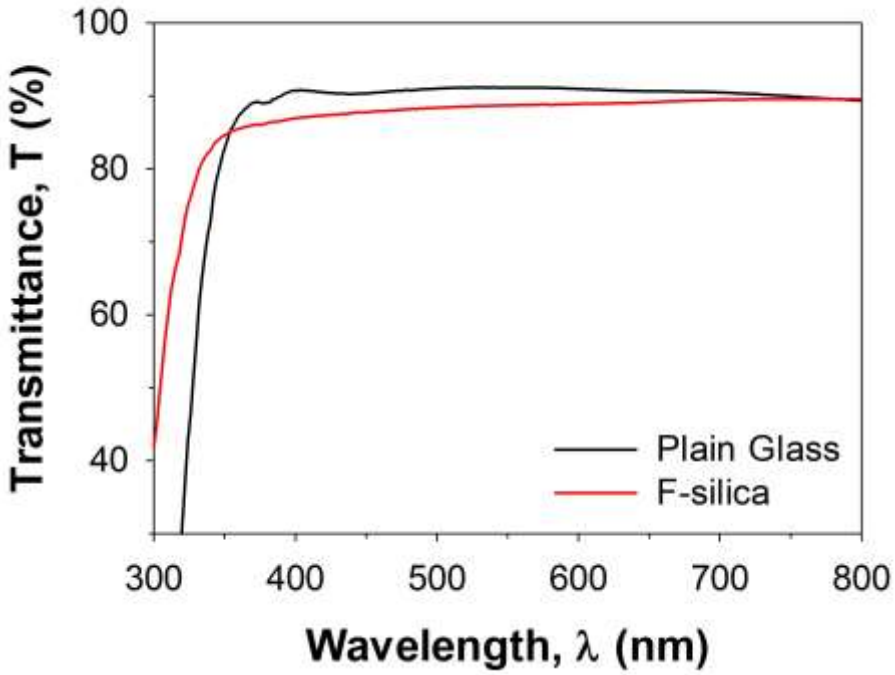

Figure S13. UV-vis transmittance analysis of fluorosilica-coated glass and plain glass in the visible light spectrum.

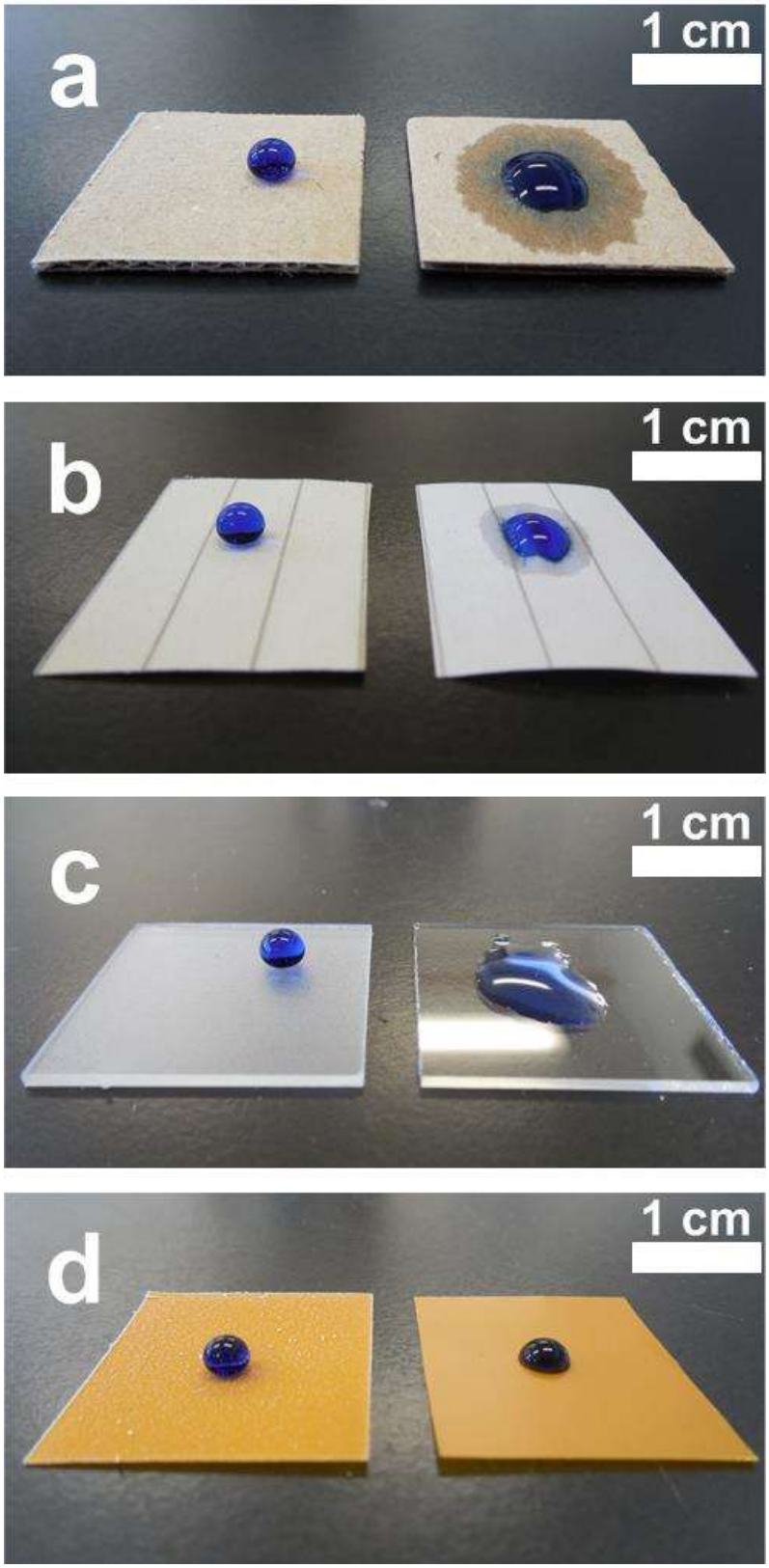

Figure S14. Multi-substrate compatibility, showing the PU-PMMA-$FSiO_2$ coating on (a) cardboard, (b) writing paper, (c) glass and (d) kapton (polyimide).

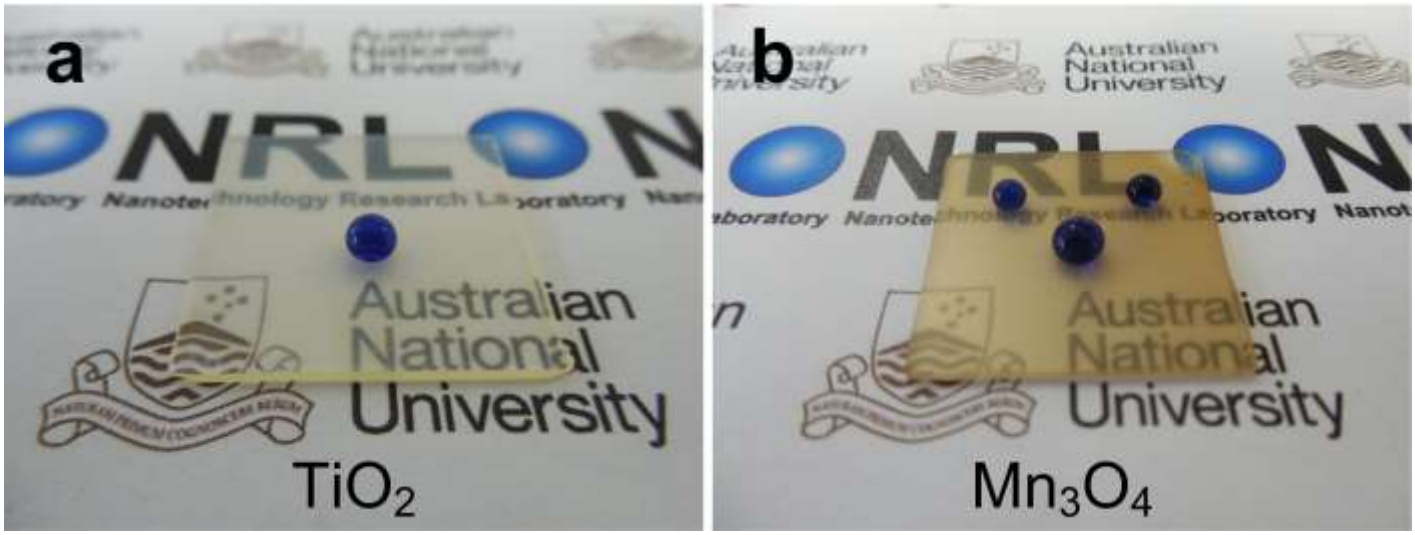

Figure S15. Suitability for alternative aerosol-based deposition methods (flame spray pyrolysis), including in-house developed superhydrophobic (a) titania and (b) manganese oxide nanoparticles. This suggests immense potential for the micro-structural conferred robustness that could be extended beyond wet-spray designs for nanoparticle-based catalytic coatings.

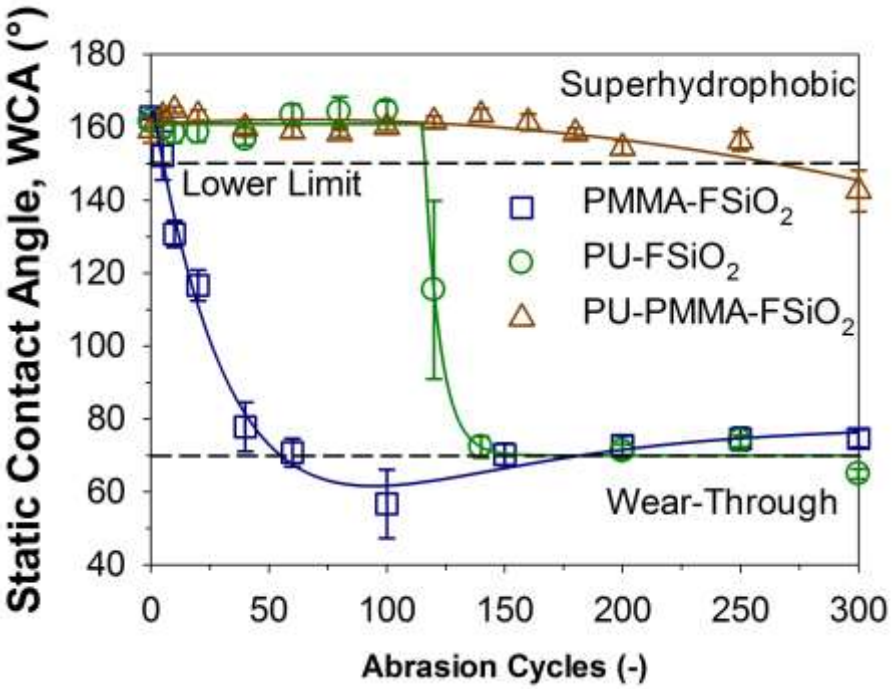

Figure S16. Tandem abrasion-wetting WCA analysis for cross-linked polymeric controls with fluoro-silica deposition versus optimized PU-PMMA-F-SiO_2 variants.

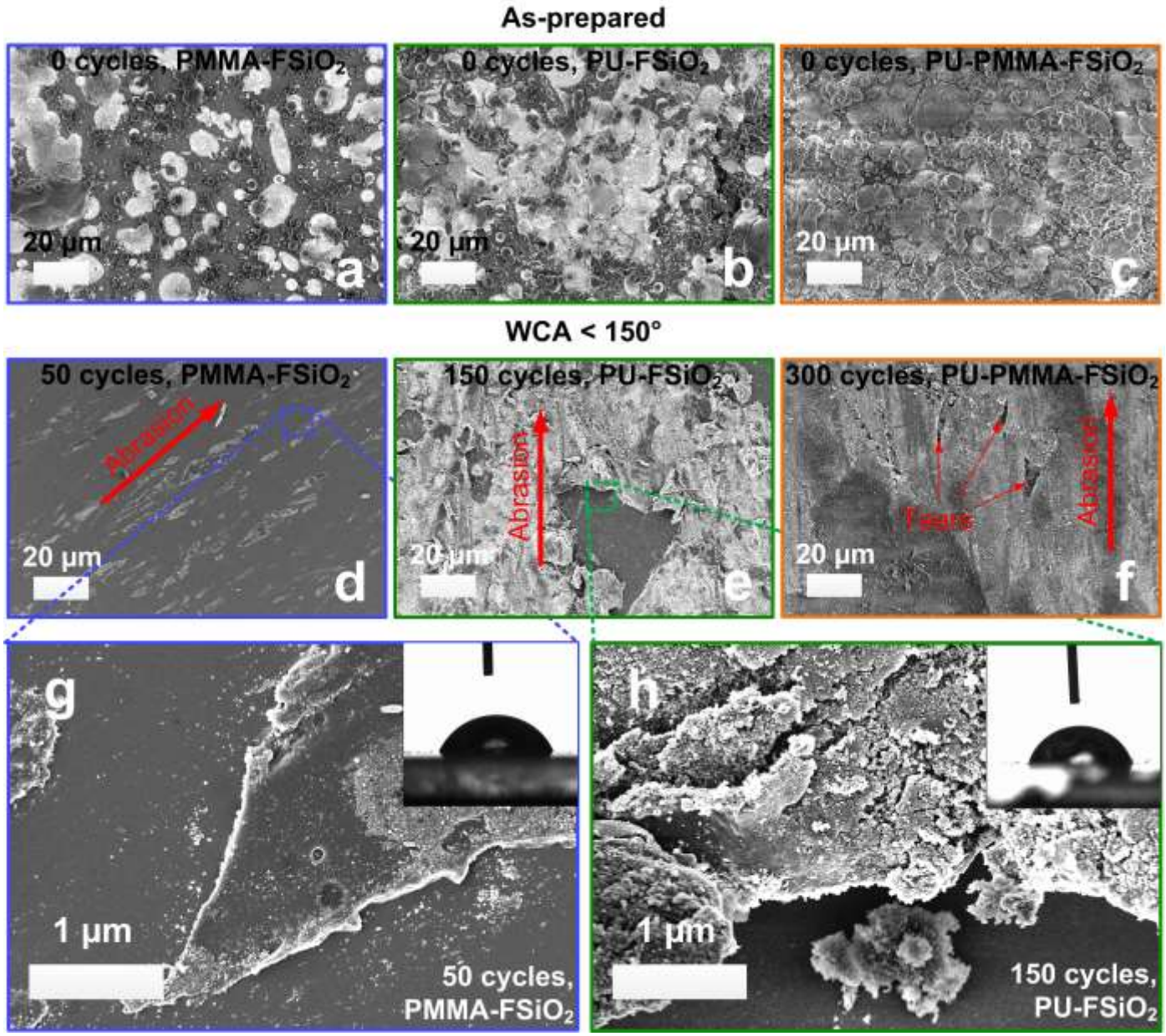

Figure S17. Low magnification SEM images of (a-c) as-prepared and (d-f) cycled-to-failure (WCA < 150°) interfaces – (a,d) PMMA-F-SiO_2, (b,e) PU-F-SiO_2 and (c,f) PU-PMMA-F-SiO_2 IPNs. High magnification SEM images showing the mode of failure (brittle and ductile) for both cross-linked (g) PMMA and (h) PU derived control coatings.

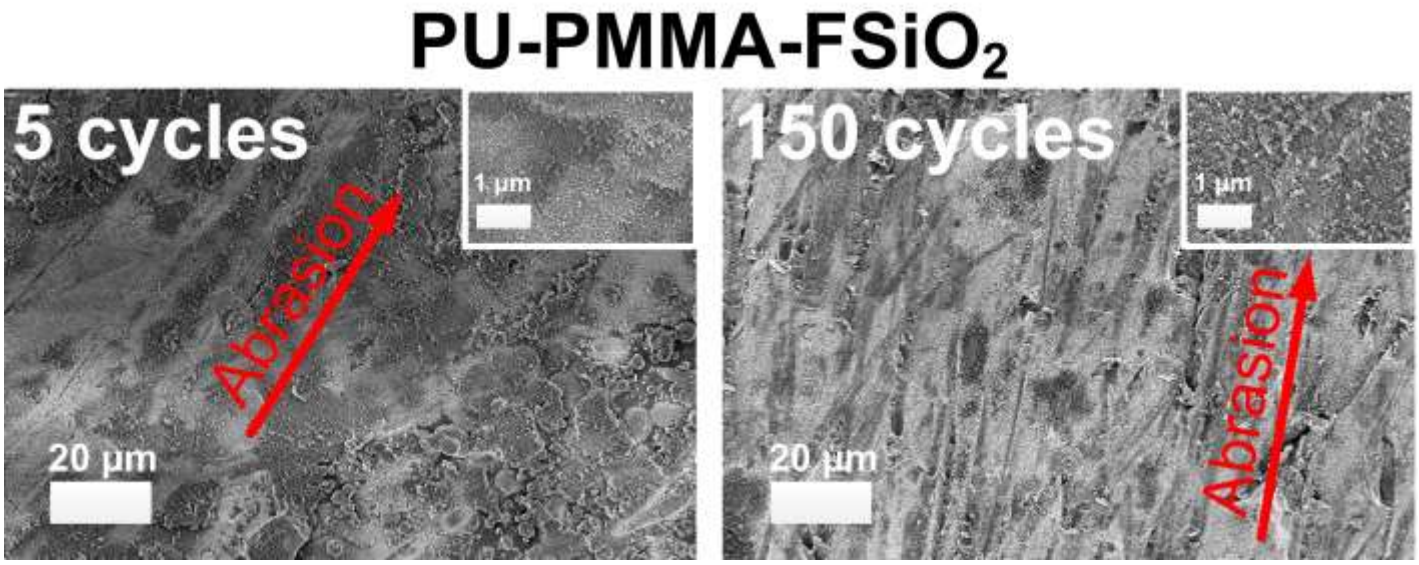

Figure S18. Intermediate cyclic damages of PU-PMMA-F-SiO_2 coatings from the 5th cycle up to the 150th cycle, with negligible damages to the IPN-F-SiO_2.

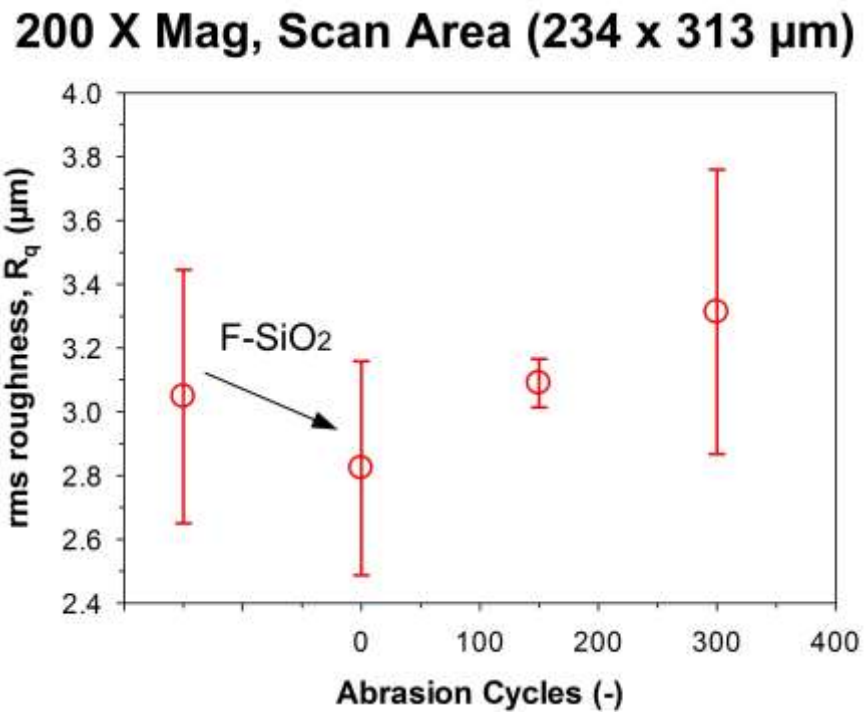

Figure S19. Impacts of F-SiO_2 coating and abrasion cycling on WLI-measured root-mean-square (rms) roughness at 200 X magnification. No trend was reasonably established in this analysis, indicative of negligible micro-level abrasion-damages.

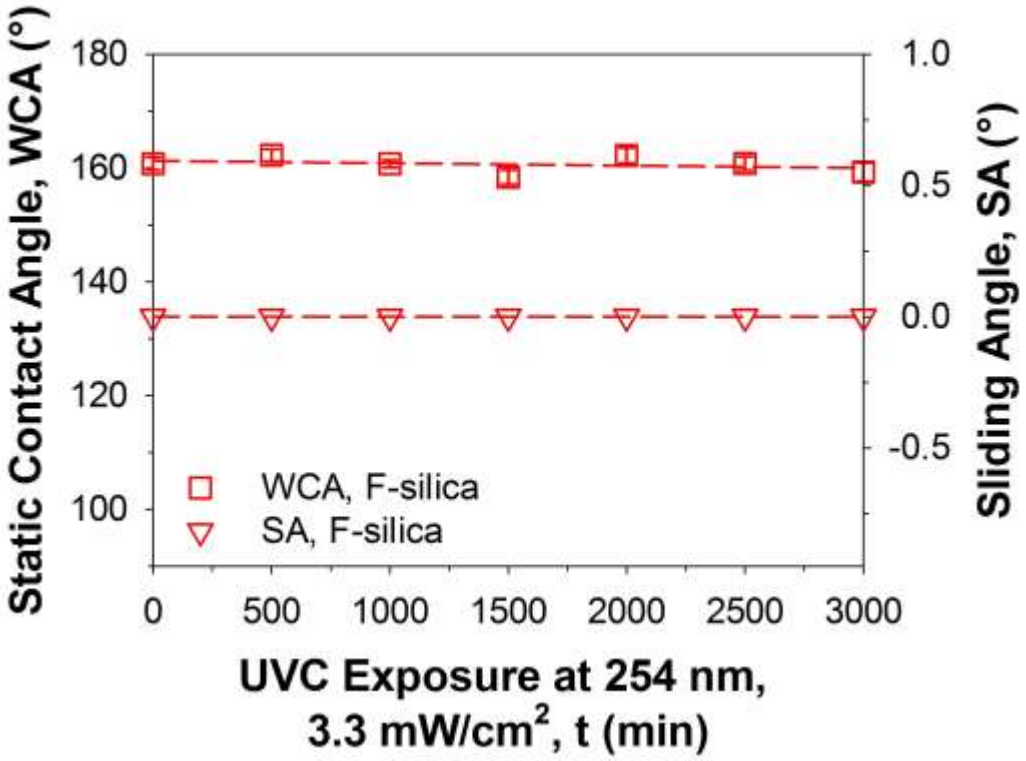

Figure S20. Stability of F-SiO_2 on glass under extended exposure to high intensity UVC.

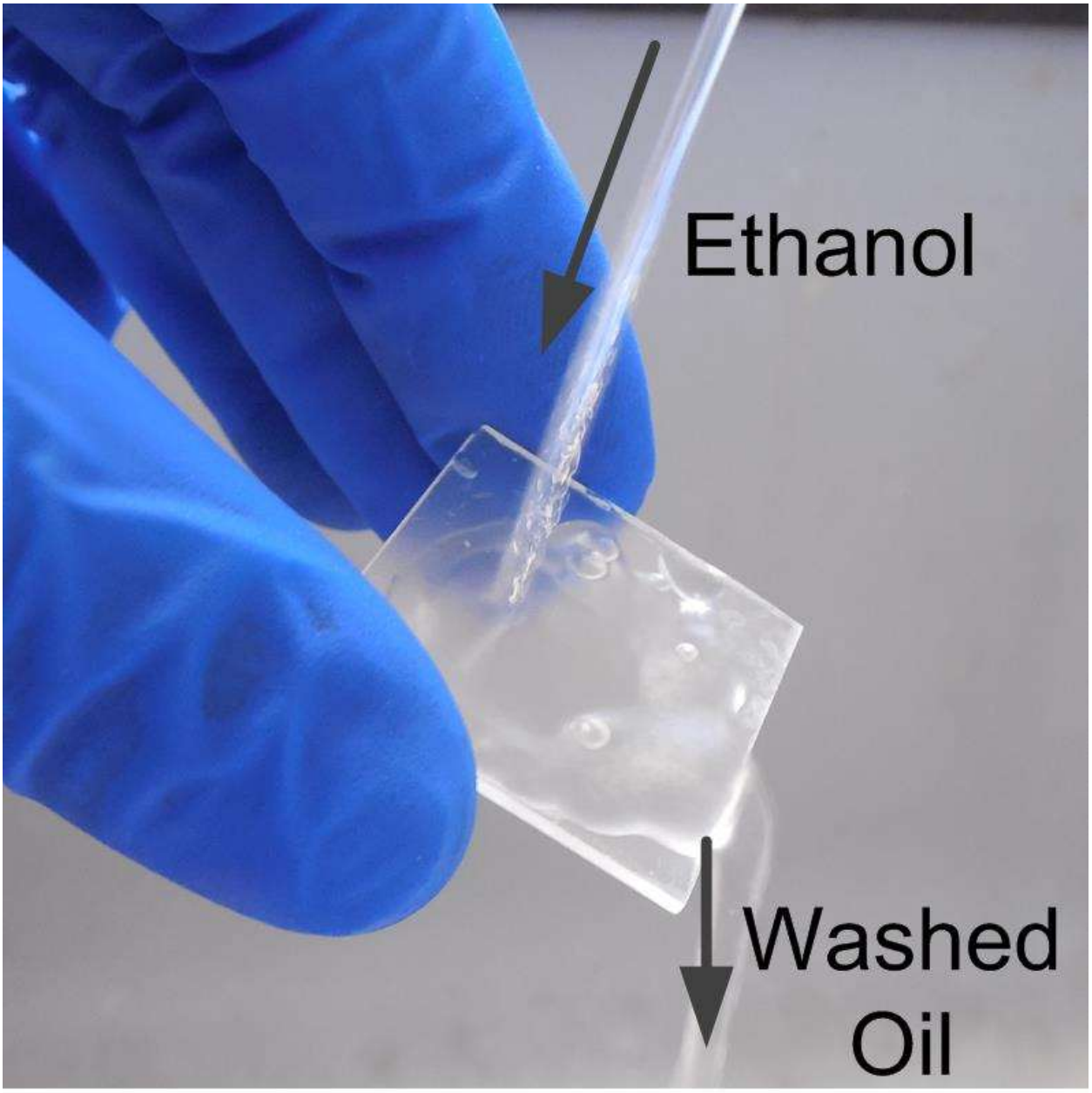

Figure S21. Ethanol decontamination of oil-immersed superhydrophobic glass slides

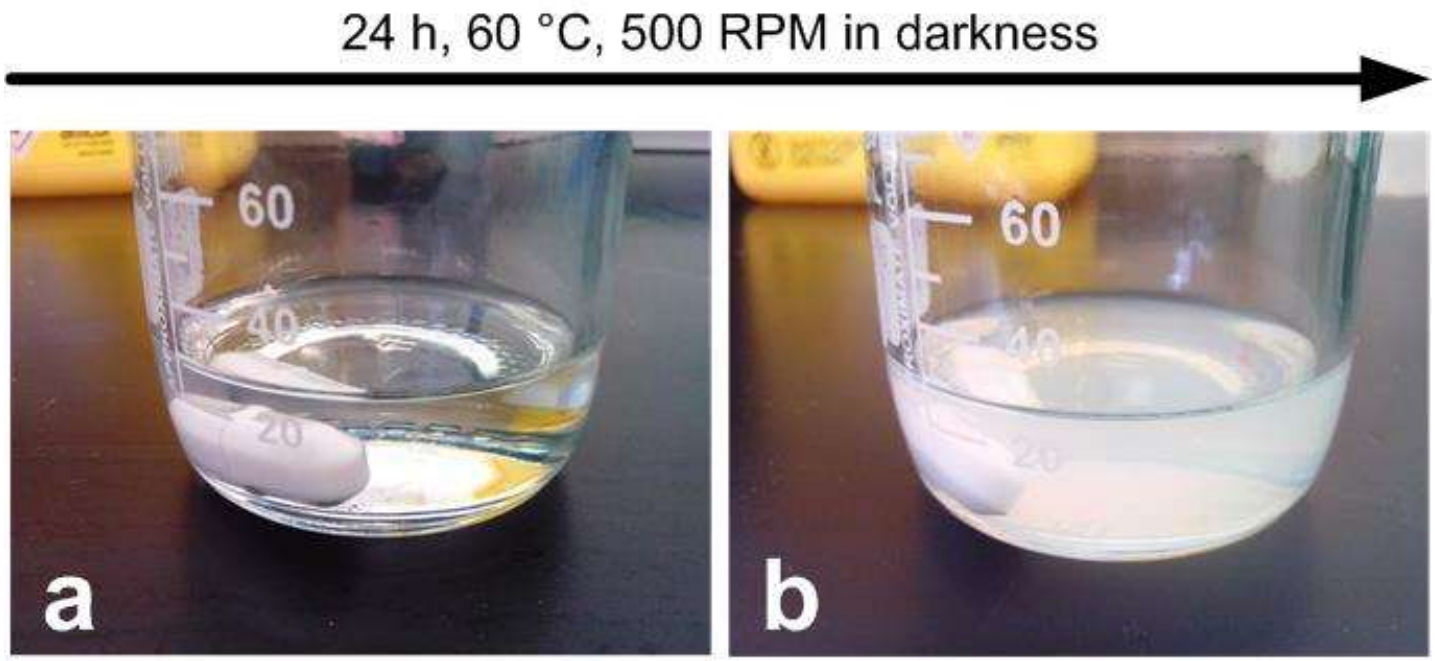

Figure S22. Reaction of (a) PU-PMMA hybrid pot to give a (b) sprayable colloidal suspension of PU-PMMA IPN solution. As-synthesized colloidal suspensions were stable for at least 6 months without any signs of settling.

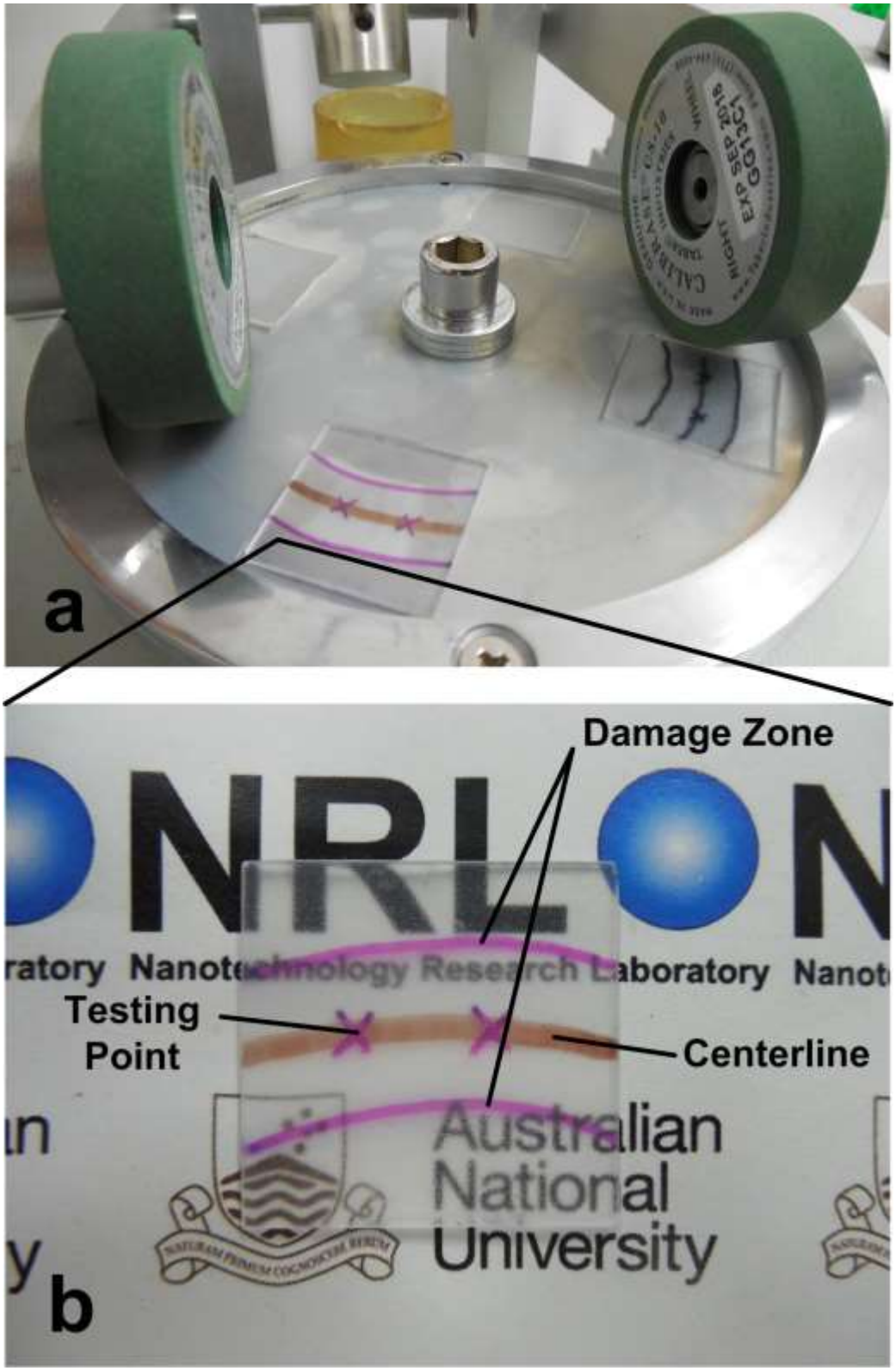

Figure S23. Cyclic (a) abrasion-wetting characterization zone (b) (along centerline).

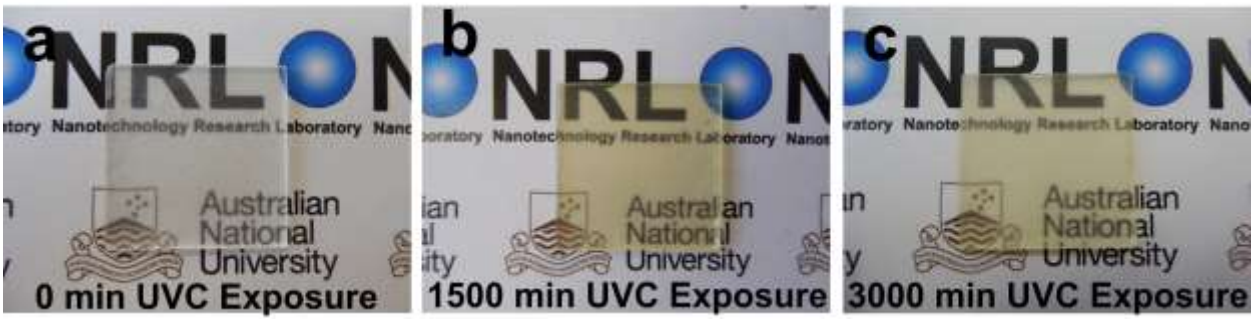

Figure S24. UVC damaged PU-PMMA-$FSiO_2$ from (a) 0 min to (b) 1500 min and (c) 3000 min exposure

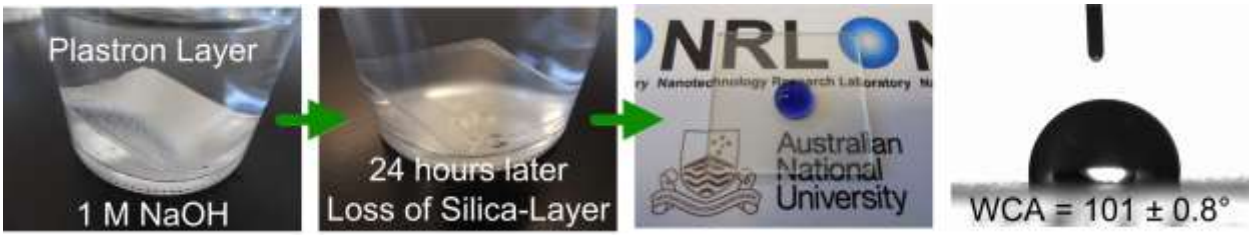

Figure S25. Alkali-induced damage of the superhydrophobic layers in the PU-PMMA-F-SiO_2 system after extended immersion. After losing its plastron layer, etching of silica occurred, leading to the loss of functionality.